6

Estimation of Induced Activity in an ADSS Facility

Nandy Maitreyee[1,*] and C. Sunil[2]
[1]*Saha Institute of Nuclear Physics, Bidhannagar, Kolkata,*
[2]*ARSS, H.P. Division, Bhabha Atomic Research Centre, Mumbai, India*

1. Introduction

In order to meet the ever growing global demand for electricity, accelerator driven subcritical systems (ADSS) are emerging as one of the preferred choices. This is due to the fact that in ADSS, the neutrons required to sustain the fission chain reaction in a reactor is supplied from spallation reaction induced by high energy protons from an accelerator, on a heavy target. The spallation target is placed in the core of the reactor. The neutrons produced are used to drive the chain reaction as well as for transmutation of radioactive waste. When the accelerator beam is turned off the supply of neutrons is stopped and any criticality accident may be averted. So ensuring safety against any type of nuclear accident is easier in these facilities as compared to the conventional power reactors. In view of this, concentrated efforts in the field of nuclear engineering are being directed towards the development of ADSS facilities. Production of high flux of fast neutrons through high energy nuclear (spallation) reactions is the main aim of the booster accelerator in an ADSS. This is achieved through the interaction of high current high energy proton beams on suitable targets. Running a high energy accelerator incurs a considerable expenditure and the accelerator parameters are decided for optimizing the cost-benefit of the system (maximum neutron yield for certain beam energy and beam current). It has been found that the neutron economy is optimized around 1 GeV proton energy [1, 2]. However, various structural parameters, target stability, heat generation profile and other logistics are studied at much lower beam energies [3], which are easily available. Running a high energy machine at high currents would lead to the generation of considerable amount of radioactive waste depending on the target-projectile combination. So, in these high current machines one of the factors constraining the beam current and irradiation time is the production of induced radio- and chemical toxicity.

Choice of the target in an ADSS facility is governed by several important factors like high neutron yield, hard neutron spectrum, low radio- and chemical toxicity, low probability of fire hazard, easy cooling of the system, high target stability, reduced cost, etc. Requirement of high neutron yield mandates a heavy element as the target material for the proton induced reaction besides demanding high current beam. Several targets were studied in this

* Corresponding Author

context. Lead and lead–bismuth alloys possess certain desirable properties which have made them to be some of the most suitable candidates for the ADSS target-coolant system [4]. Both Pb and Bi targets produce hard neutron spectrum for high energy proton induced reactions. One of the critical operating conditions of ADSS is high volumetric heat deposition rate. In this regard, Pb and Bi offer low possibility of boiling and loss of cooling, less fire-hazard (compared to liquid Na), and thereby a lower cost. Hence lead-bismuth eutectic (LBE) is one of the suitable targets for an ADSS facility. Some of the other heavy mass targets are W, U. Of these probable ADSS targets, W has similar neutron yield, while radiotoxicity of U target will be a cause of concern. In ADSS, in order to fully utilize the high energy projectile beam and to achieve the maximum neutron yield thick targets are used. In an ADSS, the projectile beam is completely stopped inside the target and maximum number of neutrons is produced from secondary interactions. So, the thickness of the target is kept much larger than the range of the projectile in the target. The amount of undesirable radionuclides produced in an ADSS giving rise to induced radioactivity depends on the target material employed, the projectile current, the transport properties of the projectile and the neutrons produced. This induced activity in ADSS target constitutes the major part of radioactive waste in the facility. The qualitative and quantitative character of this radioactive waste should be known for safe hands-on maintenance of the facility and final disposal of the used target and other materials. The nature and amount of radioactive waste that may be generated can be assessed either through experimental measurements or with the help of theoretical model based calculations. Experimental measurement is always a better choice for precision and accuracy in results, but sometimes we need to have 'a priori' estimate of the induced activity that may build up in an ADSS facility. Secondly, it is not always feasible to experimentally measure the induced activity at high energies and high currents. But, even then, the reaction models used to calculate the activity are not capable of incorporating the characteristics of all physical processes involved in the reaction. Hence the results need to be validated against experimental data.

Currently two types of target configurations are adopted for ADSS: i) windowless target and ii) target separated from the beam pipe by a thin window. Different types of stainless steel are used for the window material of which T91 and D9 are most important. Through the window the intense beam passes through and a large amount of radioactivity is induced in the window material [5]. In this paper we have estimated the radioactivity induced in an LBE target by 1 mA proton beam in the energy range of 400 MeV to 1.2 GeV. As has been mentioned earlier in this section that the neutron cost (estimated from a correlation between neutron yield and cost of running the accelerator) is minimized around 1 GeV proton energy. But the neutron yield saturates at ~2 GeV. So we have chosen the upper limit of our study at 1.2 GeV which is well suited for running an ADSS and at the same time is often affordable for relatively smaller laboratories. But the neutron yield, most often, will be higher at 2 GeV which has prompted other workers to study this energy range for characterization of ADSS parameters. It has also been mentioned earlier in this section that target stability and other studies can be carried out at a much lower energy [3]. Moreover, spallation reaction starts to predominate at proton energy of around 300 MeV. Hence we have taken the lower limit of projectile energy in this study as 400 MeV. Thus the three energies selected in our study, 400 MeV, 800 MeV and 1.2 GeV will help to understand the energy dependence of different variables studied for the ADSS employing a LBE target.

We have also estimated the activity induced in a window material of T91 or D9 stainless steel. In section 2 we describe the method of calculation with the specification of target materials, description of nuclear reaction model codes and method of calculating thick target yield of the radionuclide. In section 3 we discuss the results of our calculations.

2. Method of calculation

2.1 Specification of the target and window materials

LBE target contains 55% Bi and 45% Pb by weight. The two types of stainless steel D9 and T91 contains the naturally occurring isotopes of several elements like Fe, Cr, Mn, Mo, Ni and others. The composition of LBE, T91 and D9 are given in Table 1.

Material	Constituting Element	Weight %	Isotope (Atomic %)
LBE	Bi	55	^{209}Bi (100)
	Pb	45	^{204}Pb (1.4), ^{206}Pb (24.1), ^{207}Pb (22.1), ^{208}Pb (52.4)
T91	Fe	88.82	^{54}Fe (5.85%), ^{56}Fe (91.75%), ^{57}Fe (2.12%), ^{58}Fe (0.28%)
	Cr	9.0	^{50}Cr (4.34%), ^{52}Cr (83.79%), ^{53}Cr (9.50%), ^{54}Cr (2.37%)
	Mo	1.0	^{92}Mo (14.84%), ^{94}Mo (9.25%), ^{95}Mo (15.92%), ^{96}Mo (16.68%), ^{97}Mo (9.55%), ^{98}Mo (24.13%), ^{100}Mo (9.63%)
	Mn	0.45	^{25}Mn (100)
	Ni	0.4	^{58}Ni (68.08%), ^{60}Ni (26.22%), ^{61}Ni (1.14%), ^{62}Ni (3.63%), ^{64}Ni (0.93%)
	V	0.2	^{50}V (0.25%), ^{51}V (99.75)
	C	0.1	^{12}C (98.89), ^{13}C (1.11)
	P	0.02	^{31}P (100)
	S	0.01	^{32}S (95.02),^{33}S (0.75),^{34}S (4.21),^{36}S (0.02)
D9	Fe	63.782	^{54}Fe (5.85%), ^{56}Fe (91.75%), ^{57}Fe (2.12%), ^{58}Fe (0.28%)
	Ni	15.5	^{58}Ni (68.08%), ^{60}Ni (26.22%), ^{61}Ni (1.14%), ^{62}Ni (3.63%), ^{64}Ni (0.93%)
	Cr	14.5	^{50}Cr (4.34%), ^{52}Cr (83.79%), ^{53}Cr (9.50%), ^{54}Cr (2.37%)
	Mo	2.5	^{92}Mo (14.84%), ^{94}Mo (9.25%), ^{95}Mo (15.92%), ^{96}Mo (16.68%), ^{97}Mo (9.55%), ^{98}Mo (24.13%), ^{100}Mo (9.63%)

Material	Constituting Element	Weight %	Isotope (Atomic %)
	Mn	2.35	^{25}Mn (100)
	Si	0.75	^{28}Si (92.23),^{29}Si (4.67),^{30}Si (3.10)
	Ti	0.25	
	V	0.05	^{50}V (0.25%), ^{51}V (99.75)
	Al	0.05	^{27}Al (100)
D9	Nb	0.05	^{93}Nb (100)
	Co	0.05	^{59}Co (100)
	Cu	0.04	^{63}Cu (69.17),^{65}Cu (30.83)
	As	0.03	^{75}As (100)
	P	0.02	^{31}P (100)
	Ta	0.02	^{181}Ta (99.988)
	S	0.01	^{32}S (95.02),^{33}S (0.75),^{34}S (4.21),^{36}S (0.02)
	N	0.005	^{14}N (99.634), ^{15}N (0.366)
	B	10-20 ppm	^{10}B (19.9),^{11}B (80.1)

Table 1. Isotopic composition of LBE, T91 and D9 [5]

2.2 Source term

Radioactivity induced in the window and the target material by nuclear interaction of the high energy proton beam leads to the generation of radioactive waste. We have calculated the source term for the production of different radionuclides using two Monte Carlo nuclear reaction model codes QMD (Quantum Molecular Dynamics) [6] and FLUKA [7]. QMD calculates the production cross section for different radionuclides. From these calculated cross sections we have determined the total yield for each radionuclide in the entire target volume considering the gradual and continuous degradation of projectile energy and flux inside the target. The radiation transport code FLUKA gives the total yield of some of the radionuclides. The results obtained from the two model calculations are compared for some of the cases. The calculated results are also compared with a few experimental data.

2.3 Nuclear reaction models

2.3.1 QMD

The QMD model simulates the nuclear reaction in an event-by-event basis. Pauli exclusion principle is taken into account by forbidding collisions among the nucleons which lead to transition to already occupied or partially occupied states. The nucleons are represented by Wigner densities of Gaussian wave packets of width L of the form [6]

$$f_i(\vec{r}_i,\vec{p}_i,t)=\frac{1}{\pi h^3}\exp\left(-\frac{\left[\vec{r}_i-\vec{r}_{i0}(t)\right]^2}{2L}-\left[\vec{p}_i-\vec{p}_{i0}(t)\right]^2\frac{2L}{h^2}\right) \quad (1)$$

r_{i0} and p_{i0} are the centroids of position and momentum of the ith nucleon. The distribution function for the total system is given by

$$f_i(\vec{r},\vec{p},t) = \sum_i f_i(\vec{r}_i,\vec{p}_i,t)$$

The time evolution of r_i and p_i is described by,

$$\begin{aligned} \frac{d}{dt}(\vec{r}_i) &= \{H_i,\vec{r}_i\} \\ \frac{d}{dt}(\vec{p}_i) &= \{H_i,\vec{p}_i\} \end{aligned} \tag{2}$$

where H is the Hamiltonian for the system. H consists of kinetic energy, Skryme, Coulomb, Yukawa interaction part and the symmetry energy. Transition between equilibrium, pre-equilibrium and spallation mechanisms including fast multi-particle emissions is effected by changing the relative importance of mean field effects and nucleon-nucleon collisions. Non-equilibrium emissions which play an important role in high energy reaction have been taken into account [2].

The QMD theory considers realistic momentum distribution of the nucleons inside the nucleus, multistep process, multiple pre-equilibrium emission process and variation of the mean field potential due to excitation. Time evolution of r_i and p_i are determined from eqs (2). Particle trajectory is followed through the nuclear volume and once a particle escapes the nuclear boundary, emission is considered. If the positions and momenta of some particles lie within a previously defined range, they are considered to form a cluster. A statistical decay model (SDM) is employed to estimate evaporation from residual nuclei following fast particle emissions as estimated by the QMD model.

QMD calculates the production cross section of different nuclides. The reaction cross section of the projectile in the target calculated by the code is not explicitly expressed. In absence of such information we have used the value of the maximum impact parameter (b_{max}) to approximate the reaction cross section and determine the degradation of projectile flux inside the thick target. The reaction cross section (σ_r) is calculated by,

$$\sigma_r = \pi b_{\max}^2 \left(1 - \frac{B_C}{E_p}\right) \tag{3}$$

where B_C is the Coulomb barrier for the reaction and E_p is the projectile energy

2.3.2 FLUKA

FLUKA [7] is a general purpose tool for calculation of particle transport and interactions with matter, covering an extended range of applications spanning from proton and electron accelerator shielding to target design, calorimetry, activation, dosimetry, detector design, Accelerator Driven Systems, cosmic rays, neutrino physics, radiotherapy etc. It can simulate the interaction and propagation of 60 different types of particles from electrons, photons, neutrons to optical photons, neutrinos, muons etc., most of them of energy from as low as few keV to several TeV. The code has the latest physics models incorporated and is constantly being updated with the latest available data. It can handle even very complex geometries, using an improved version of the well-known Combinatorial Geometry (CG)

package. Several user routines are available for very advanced scoring and tracking of particles of interest.

FLUKA(2011) Monte Carlo code was used to calculate the induced activity production in the LBE column. The irradiation profile card (IRRPROFI) allows the flexibility of switching on and off constant beam currents for several intervals and can simulate the irradiation condition with in-between temporary shut offs. This card was used to simulate a constant irradiation of the LBE by a 1 mA beam current for a period of one month. A cylindrical LBE target was chosen as the geometry for irradiation. The length of the cylinder was kept more than the range of the proton (calculated using the SRIM [8] code) while the diameter was fixed at 30 cm to take care of the lateral hadronic cascade. RESNUCLE card was used to calculate the residual nuclei production. For accurate results the new evaporation, heavy fragment evaporation and coalescence modules were activated with the PHYSICS card. Heavy recoils too, were transported using the IONTRANS option as stipulated in the manual. Radioactive decay was requested through the RADDECAY card while induced activity was calculated at different cooling times defined by the DCYTIMES and associating one RESNUCLE cards for every cooling time using the DCYSCORE card. The results were obtained in the units of Bq cm^{-3} and were converted using the volume of the target.

2.4 Thick target calculation

The transport code FLUKA gives the total yield of radionuclides in a thick target while the nuclear reaction model code QMD calculates the production cross section of the radioisotopes. From the production cross sections generated by QMD, total yields of different radioisotopes were calculated by adopting a conservative approach. The total thickness of the target is such that the projectile is completely stopped in the target. It has been considered that the thick target is made of a number of thin slabs, such that the projectile loses equal amount of energy, ΔE, in each of these slabs. Energy lost by the projectile per unit path length or the stopping power is calculated using the code SRIM [8]. The total yield of a radionuclide produced is the sum of yields of that particular nuclide from all of the thin slabs at gradually degrading projectile energy weighted by the properly attenuated projectile flux. Moreover it is assumed that the scattering and absorption of the neutrons produced by the primary interaction of the proton beam is negligible. The neutrons produced also contribute to the production of some of the radioisotopes responsible for augmentation of the final repository of the radionuclides.

The kinetic energy E^i_P of the projectile incident on the i-th slab and the slab thickness x_i are, respectively, given by [9,10],

$$E_p^i = E_p^0 - (i-1)\Delta E$$

$$x_i = \int_{E_p^i}^{E_p^{i+1}} \frac{dE}{-dE/dx}$$

where E^0_p is the incident energy. Using this formalism we estimated the yield and activity of radionuclides from calculated formation cross sections in the QMD code.

3. Results and discussion

We have used reaction model codes to estimate the activity induced in LBE, T91 and D9 targets. Since the reaction model codes use several approximations and cannot incorporate all the detailed features of nuclear reactions, these codes need to be validated against experimental data. We have compared a few experimentally measured cross sections for formation of nuclides by proton induced reaction on Pb and Bi target with those obtained from QMD calculations. This comparison is shown in Table 2. From Table 2 we see that the measured cross sections are fairly reproduced by the calculated values in the energy range considered. We have not compared the cross section calculated by FLUKA with measured data in this work, but the code has already been well validated.

Reaction	Energy (MeV)	Cross section (mb)	
		Experiment	QMD
^{nat}Pb (p, X)^{200}Tl	660	28.0 ± 8 [11]	17.0
^{nat}Pb (p, X)^{198}Au	660	1.8 ± 0.3 [11]	2.7
^{209}Bi(p,7n5p)^{198}Au	1500	0.4 ± 0.1 [12]	1.0

Table 2. Comparison of experimentally measured [11,12] and QMD calculated cross sections for a few nuclides

Z	A	Nuclide	Half-life	Radiation	γ energy (MeV)
1	3	^{3}H	12.33 y	β–	
6	14	^{14}C	5730 y	β–	
11	22	^{22}Na	2.6 y	ε	0.511, 1.27
11	24	^{24}Na	14.96 y	β–	
19	40	^{40}K	1.277e+9 y	β–, γ	1.46
20	45	^{45}Ca	162.61 d	β–	
27	60	^{60}Co	1925.1 d	γ	1.17, 1.33
53	125	^{125}I	59.408 d	ε	
53	126	^{126}I	13.11 d	ε, β–	
53	131	^{131}I	8.02 d	β–	0.364
54	127	^{127}Xe	36.34 d	ε	
55	131	^{131}Cs	9.689 d	ε	
55	132	^{132}Cs	6.479 d	ε, β–	
55	134	^{134}Cs	2.0648 y	β–	0.136, 0.475
56	131	^{131}Ba	11.5 d	ε	0.123, 0.216, 0.496
56	133	^{133}Ba	3854 d	ε	0.303, 0.356, 0.383
57	140	^{140}La	1.678 d	β–	0.487
78	188	^{188}Pt	10.2 d	ε, α	

Z	A	Nuclide	Half-life	Radiation	γ energy (MeV)
78	190	^{190}Pt	6.5e+11 y	α	
78	191	^{191}Pt	2.96 d	ε	
79	195	^{195}Au	186.1 d	ε	0.261
79	196	^{196}Au	6.183 d	ε, β–	0.333, 0.355
80	194	^{194}Hg	520 y	ε	
80	197	^{197}Hg	64.14 h	ε	0.077
80	203	^{203}Hg	46.612 d	β–	0.279
81	200	^{200}Tl	26.1 h	ε	
81	201	^{201}Tl	72.91 h	ε	0.167
81	202	^{202}Tl	12.23 d	ε	
81	204	^{204}Tl	3.78 y	β–, ε	0.439
82	202	^{202}Pb	52.5e3 y	ε	0.422, 0.787, 0.96
82	203	^{203}Pb	51.873 h	ε	0.279, 0.401
82	205	^{205}Pb	1.53e7 y	ε	
83	205	^{205}Bi	15.31 d	ε	
83	206	^{206}Bi	6.243 d	ε	
83	207	^{207}Bi	31.55 y	ε	0.569, 0.894, 1.43,
83	208	^{208}Bi	3.68e+5 y		0.51, 0.65, 0.921

Table 3. Half-life and radiation type of radionuclides for which activity is estimated after 30 days of irradiation [13]

In this work, we have studied the activities of various radionuclides produced, for 30 days of irradiation, due to proton induced reactions on LBE target in the projectile energy range of 400 MeV to 1.2 GeV at a beam current of 1 mA. Induced activities of nuclides calculated using QMD and FLUKA are reported. The list of radionuclides along with their half-lives and type of radiation emitted are given in Table 3. The neutrons produced in the primary interaction also contribute to activity build-up for nuclides near the target mass range. But this has not been taken into account in the QMD calculations. Activity of different radionuclides is estimated for continuous irradiation ranging from 1 day to a maximum period of 30 days. In calculating the induced activity in LBE target we have considered the target thickness to be sufficiently larger than the range of the proton in LBE at the incident projectile energy. As a result the radioactivity induced by the primary projectile has become independent of the target volume.

In figures 1 to 4 we have shown the activity of radionuclides in the mass range of 3 to 208 formed due to proton induced reactions on LBE for 400 MeV, 800 MeV and 1.2 GeV calculated using the code QMD. The radionuclides considered are those having half-lives of more than several days. In some of the cases the product radionuclide may be formed either in the ground state or in a metastable state. Since the codes do not distinguish between formation in the ground or metastable state, in the case of such radionuclides, we have considered the half-life of the ground state unless the metastable state is much longer lived than the ground state. Figure 1 shows the activity build-up of ^{3}H, ^{14}C, $^{22, 24}$Na, ^{45}Ca and ^{60}Co.

^{3}H, ^{45}Ca and ^{60}Co are nuclides of concern for radiotoxicity of the environment while ^{14}C and ^{22}Na are biologically important. It has been observed that for 400 MeV incident proton energy the activity build-up for 30 days of irradiation is in the range of 10^{10} to $2x10^{11}$ Bq for all the species except for ^{14}C. Maximum activity of the order of $2.3x10^{11}$ Bq is produced for ^{45}Ca. ^{14}C is a much longer lived isotope than the other product nuclides shown here. The reaction system considered in this plot produces an activity of ~$2x10^{7}$ Bq for ^{14}C.

As we go to higher projectile energies the variation in the activity build-up pattern with nuclide species changes for the same mass range. In figure 1b we see that for 800 MeV proton energy maximum activity of the order of ~ $8.8x10^{11}$ Bq is obtained for ^{3}H while ^{45}Ca activity is slightly less (~ $7.0x10^{11}$ Bq). At the highest energy 1.2 GeV of the entire energy range considered ^{3}H still have maximum activity of $2.3x10^{12}$ Bq while ^{45}Ca has a slightly lower activity of $6.3x10^{11}$ Bq than that at 800 MeV. This observation is explained from the fact that as we go to higher energies, production of high energy neutrons and projectile-like fragments increase [14, 15], competition between a larger number of evaporation channels also come into play [5]. It has been observed from figure 1 that for the nuclide species and the energy range considered, saturation activity is not reached for any of the products for 30 days of irradiation.

Figures 2 (a), (b) and (c) show the activity build-up of different radionuclides in the mass range of 125 to 140. ^{125,131}I are biologically important radionuclide as they are used for diagnosis and therapy of thyroid malfunction, Cs is a bone seeking element, radioactive Xe adds to the radiotoxicity of the environment while Ba and La are important lanthanides. From figure 2 we observe that at 400 MeV beam energy maximum activity is obtained for ^{132}Cs which is of the order of $1.9x10^{12}$ Bq while minimum activity (~$1.2x10^{10}$ Bq) is obtained for ^{134}Cs which is a very long lived isotope. At 800 MeV projectile energy the trend of the activity build-up changes and maximum activity is produced for ^{131}Ba while ^{132}Cs is produced with an activity less than that by 7.7%. Activity of ^{134}Cs is higher (~$3.6x10^{10}$ Bq) than the minimum activity of the order of $1.6x10^{10}$ Bq obtained for ^{133}Ba. At 1.2 GeV, variation of induced activity formation with nuclide species again changes and ^{140}La is produced with maximum activity of ~ $3.0x10^{12}$ Bq. Minimum activity at this energy is obtained with ^{133}Ba. It has also been observed that for the mass range considered in figure 2 and for 30 days of irradiation, saturation activity is reached only ^{140}La at 800 MeV and 1.2 GeV beam energy, while at 400 MeV no significant activity of ^{140}La is produced.

In figures 3 (a), (b) and (c) we have plotted the induced activity of some radionuclides in the noble metal group and Hg for 400, 800 MeV and 1.2 GeV proton induced reaction on LBE. From these figures we see that for the isotopes of Pt, Au and Hg shown, the magnitude of maximum activity obtained is much larger than the other two mass groups studied. Maximum activities of $3.2x10^{13}$ Bq, $4.0x10^{13}$ Bq, $3.4x10^{13}$ Bq, respectively, are produced for ^{197}Hg for the three beam energies considered while minimum activity is achieved for ^{194}Hg. In this mass region saturation activity is obtained for ^{194}Au and ^{197}Hg. In figures 4 (a), (b) and (c) we have plotted the activities produced for nuclides close to the target nuclides. From this figure it has been observed that for the entire mass range of product nuclide considered maximum activity is obtained for ^{203}Pb and ^{200}Tl. These activities attain the highest value at 800 MeV and are of the order of $5.5x10^{13}$ Bq and $6.5x10^{13}$ Bq, respectively. Activity produced for ^{201}Tl in 30 days' irradiation is similar to that for ^{200}Tl at 400 MeV, but at 800 MeV and 1.2 GeV proton energy, these are less than the induced activity of ^{200}Tl by 27% and 15% respectively.

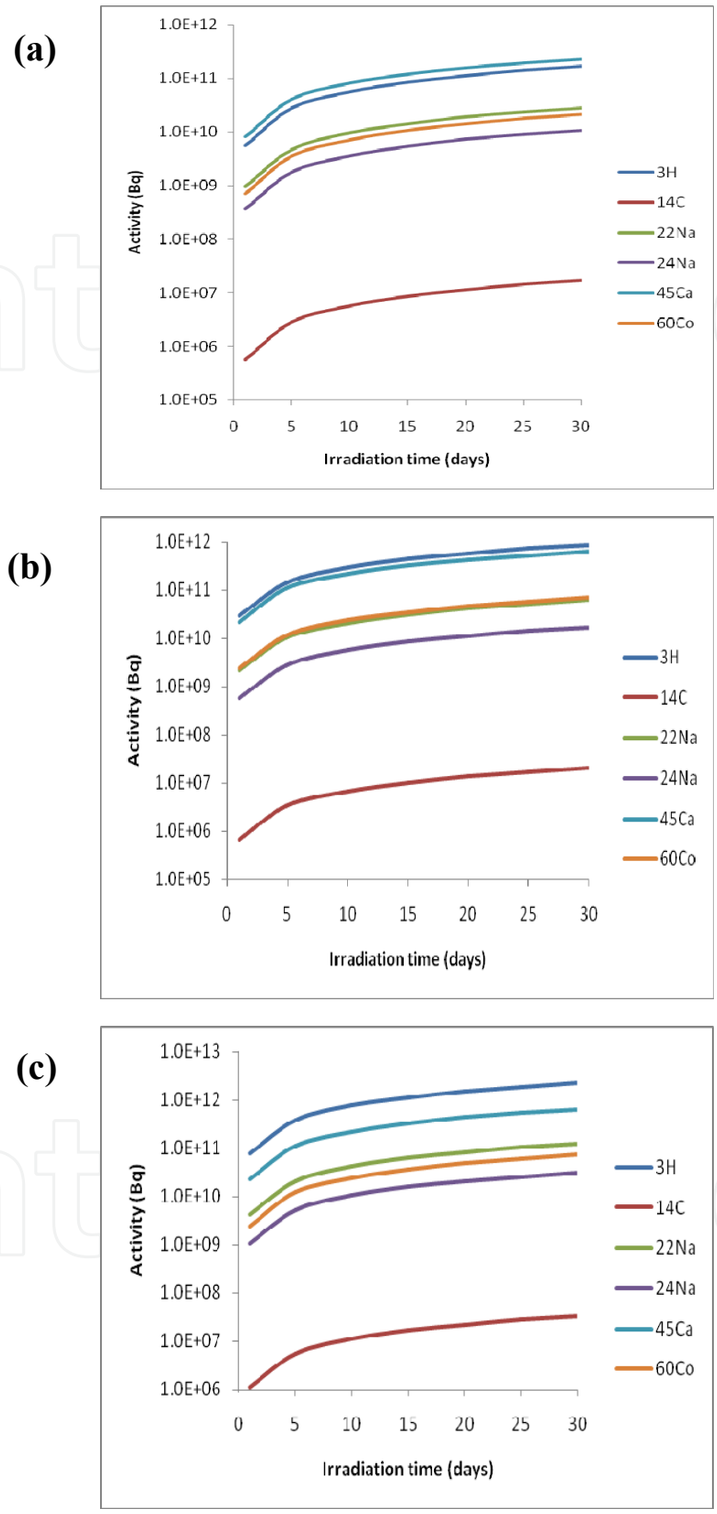

Fig. 1. Activity build-up of some radionuclides in the mass range 3 – 60 for 1 mA proton beam induced reaction on LBE target at beam energy of (a) 400 MeV, (b) 800 MeV and (c) 1.2 GeV

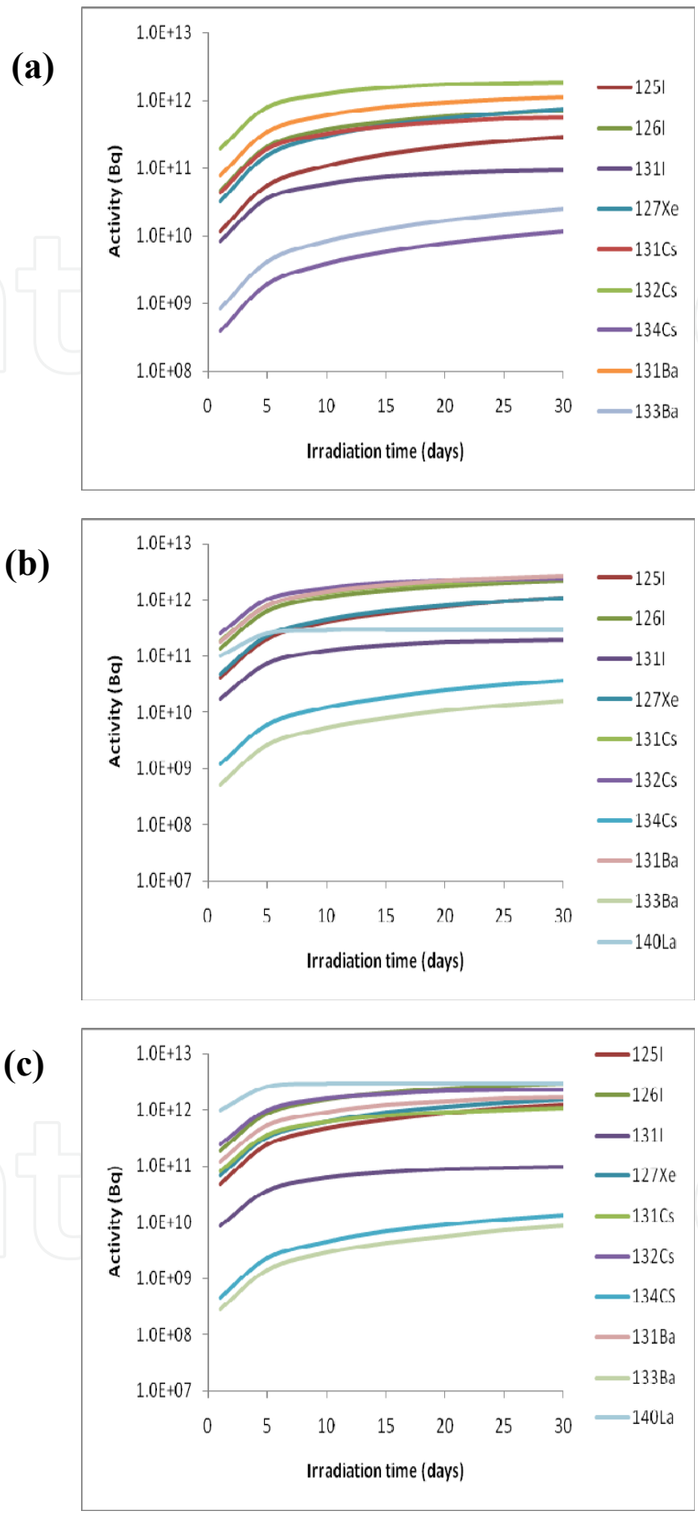

Fig. 2. Activity build-up of some radionuclides in the mass range 125 –140 for 1 mA proton beam induced reaction on LBE target at beam energy of (a) 400 MeV, (b) 800 MeV and (c) 1.2 GeV

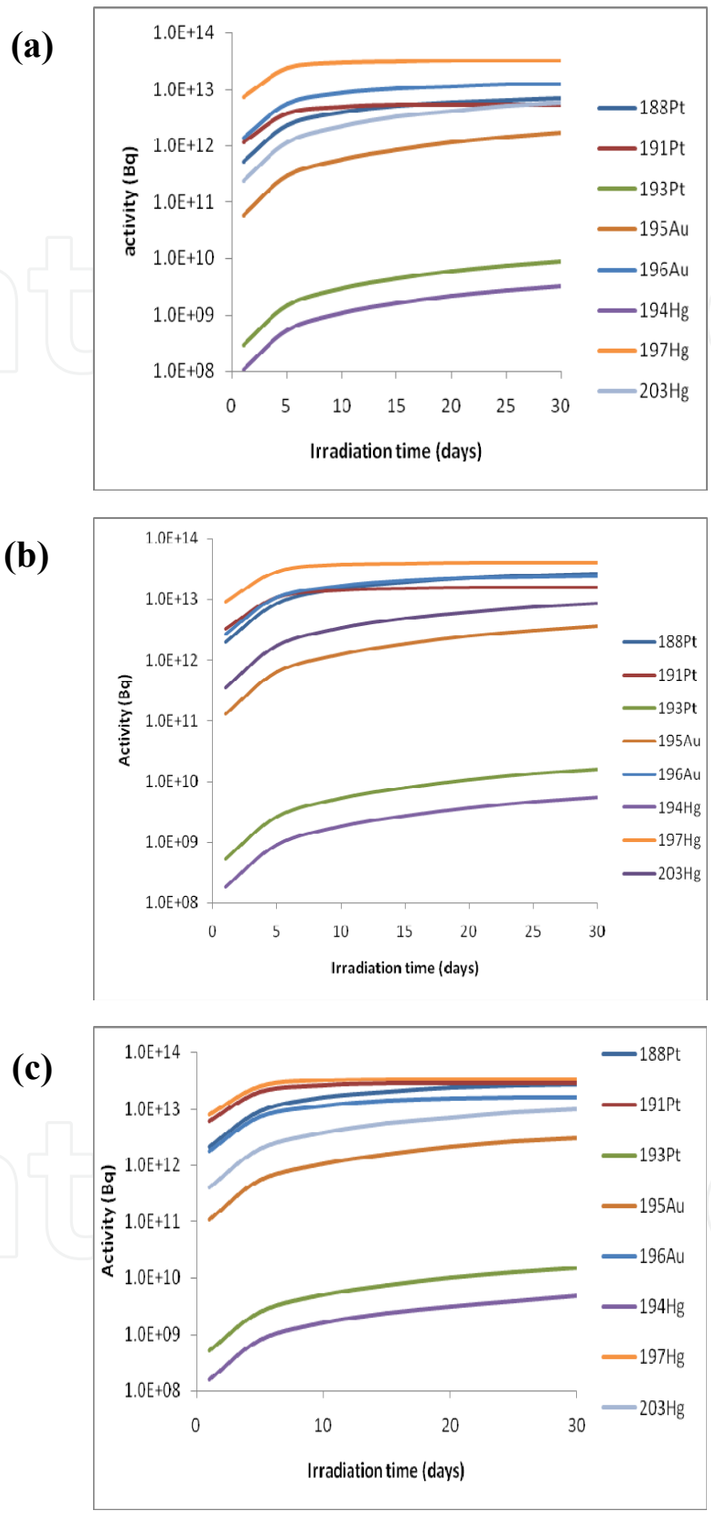

Fig. 3. Activity build-up of some radionuclides in the mass range 188 – 203 for 1 mA proton beam induced reaction on LBE target at beam energy of (a) 400 MeV, (b) 800 MeV and (c) 1.2 GeV

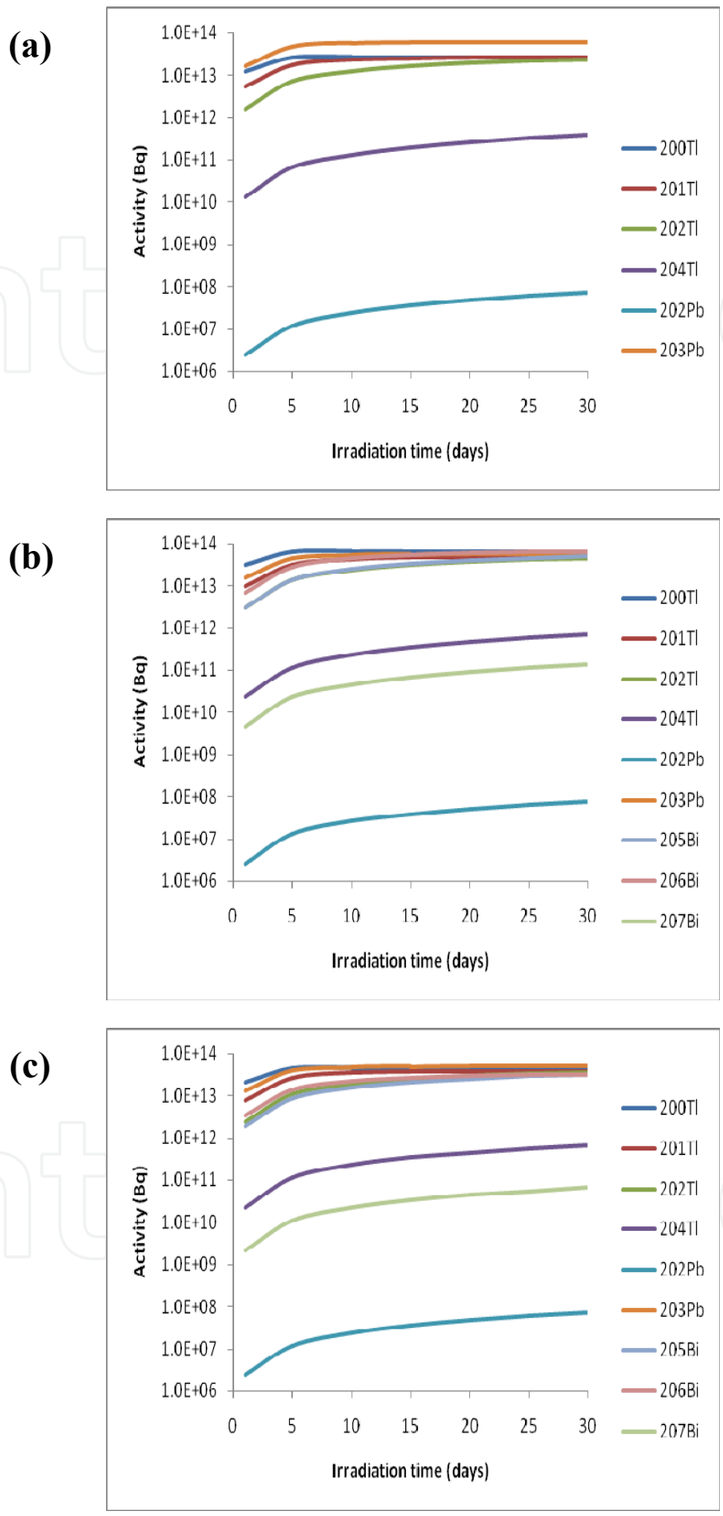

Fig. 4. Activity build-up of some radionuclides in the mass range 200 – 207 for 1 mA proton beam induced reaction on LBE target at beam energy of (a) 400 MeV, (b) 800 MeV and (c) 1.2 GeV

We have also calculated the activity of various radionuclides produced in proton induced reaction on LBE target in the energy range from 400 MeV to 1.2 GeV using the code FLUKA. In Table 4 we have given these calculated activities of several radionuclides for proton energies of 600 MeV and 1.0 GeV. From the table we see that for both the projectile energies considered maximum activities of the order of 6.0×10^{14} Bq and 1.0×10^{15} Bq, respectively are obtained for ^{201}Tl while minimum activity is produced for ^{205}Pb. This minimum activity is of the order of 3.6×10^{6} Bq and 7.7×10^{6} Bq respectively. It has also been observed that saturation activities are reached for ^{191}Pt, ^{196}Au, ^{197}Hg, ^{200,201}Tl, ^{203}Pb. Our analysis revealed that the activity induced for various radionuclides after 30 days of irradiation as calculated by FLUKA is underpredicted to a small extent by the QMD calculation. This is explained from the fact that FLUKA simulations also take into account the activation of the target nuclei by the neutrons produced in primary interaction besides activation by the primary projectile. But in QMD calculation we have not included the production of radionuclides by neutrons.

In figures 5 and 6 we have shown the yield of different nuclides plotted against atomic number Z and mass number A for proton energy 600 MeV and 1.0 GeV, respectively. In fig. 5 we see that in the mass range upto A=150, yield of most of the nuclides are in the range of 10^{11} atoms. Some of the nuclides in the range Z= 40 – 50 and A = 100 – 125 are produced with a yield of 10^{14} atoms. But as we approach nearer to the target mass region the yield of nuclides increases to ~ 10^{15} – 10^{16} atoms. At projectile energy of 1.0 GeV this general trend of variation of yield for different species of nuclides remain the same, but the absolute yield of the nuclides increase, particularly for higher mass nuclides. The maximum yield of the target like nuclides is of the order of 10^{16}.

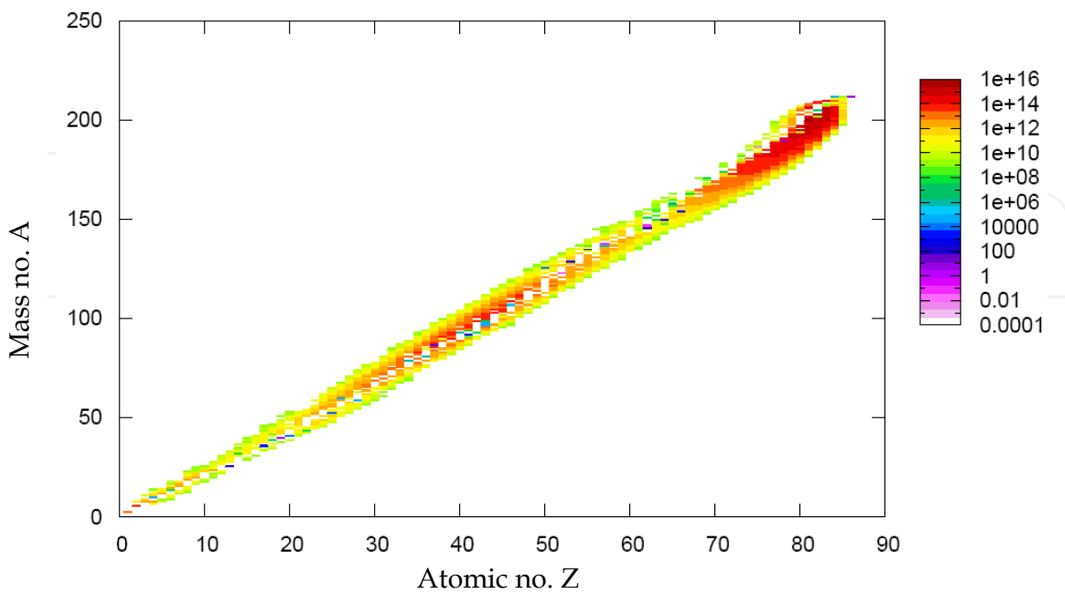

Fig. 5. Yield of nuclides for 1 mA, 600 MeV proton irradiation of LBE target for 30 days, plotted against atomic no. Z and mass no. A

A	Z	Nuclide	Activity (Bq) for proton energy (MeV)	
			600 MeV	1.0 GeV
208	83	^{208}Bi	2.5E+08	5.8E+08
205	82	^{205}Pb	3.62E+06	7.70E+06
203	82	^{203}Pb	7.7E+14	1.4E+15
202	82	^{202}Pb	7E+08	1.2E+09
204	81	^{204}Tl	1.1E+12	2.2E+12
202	81	^{202}Tl	8E+13	1.6E+14
201	81	^{201}Tl	6E+14	1E+15
200	81	^{200}Tl	5.3E+14	8.8E+14
203	80	^{203}Hg	1.9E+12	4.4E+12
197	80	^{197}Hg	3E+14	4.8E+14
194	80	^{194}Hg	2.3E+10	3.6E+10
196	79	^{196}Au	2.3E+12	6E+12
195	79	^{195}Au	2.4E+13	3.7E+13
193	78	^{193}Pt	2.4E+11	3.9E+11
191	78	^{191}Pt	9.8E+13	1.8E+14
188	78	^{188}Pt	6.2E+13	1.3E+14
60	27	^{60}Co	6.9E+09	2E+10
45	20	^{45}Ca	1.8E+10	7.6E+10
24	11	^{24}Na	4.5E+11	1.8E+12
22	11	^{22}Na	3.7E+08	2E+09
14	6	^{14}C	2E+07	9E+07
3	1	^{3}H	3.3E+12	8E+12

Table 4. Activity of radionuclides after 30 days of irradiation as calculated by FLUKA for 600 MeV and 1.0 GeV proton induced reaction on LBE target.

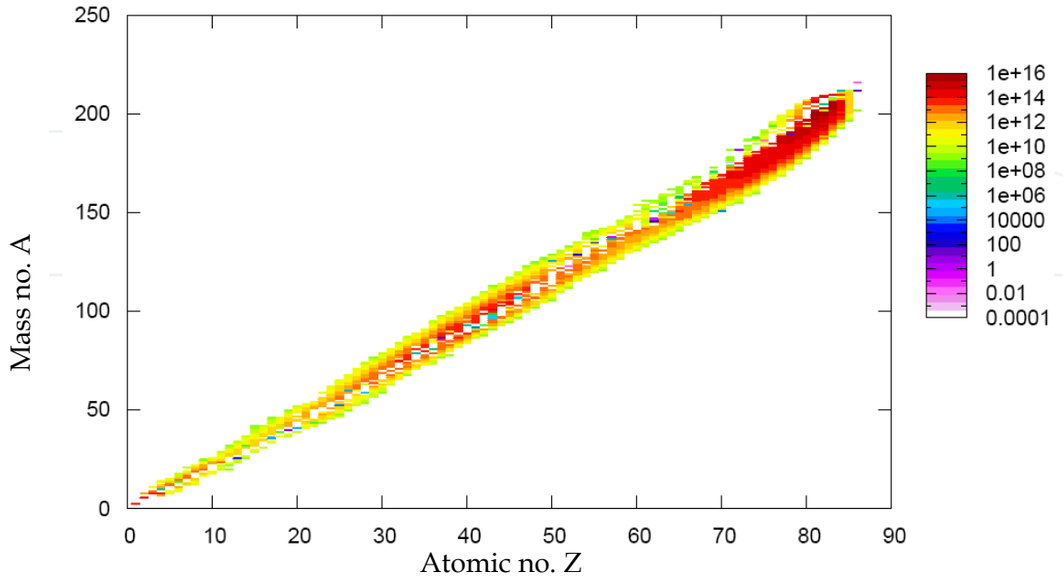

Fig. 6. Yield of nuclides for 1 mA, 1000 MeV proton irradiation of LBE target for 30 days, plotted against atomic no. Z and mass no. A

In the case of LBE target irradiated by a proton beam, one of the major concern on radiotoxicity is the production of ^{210}Po via the production of β– emitter ^{210}Bi by neutron induced reaction. ^{210}Po is an α emitter and pose a potential hazard for internal contamination. We have estimated the production and decay of ^{210}Po using the code FLUKA. Figure 7 shows the activity of ^{210}Po over cooling times of 10^2 sec to 10^7 sec after beam shutdown at the end of 30 days of irradiation.

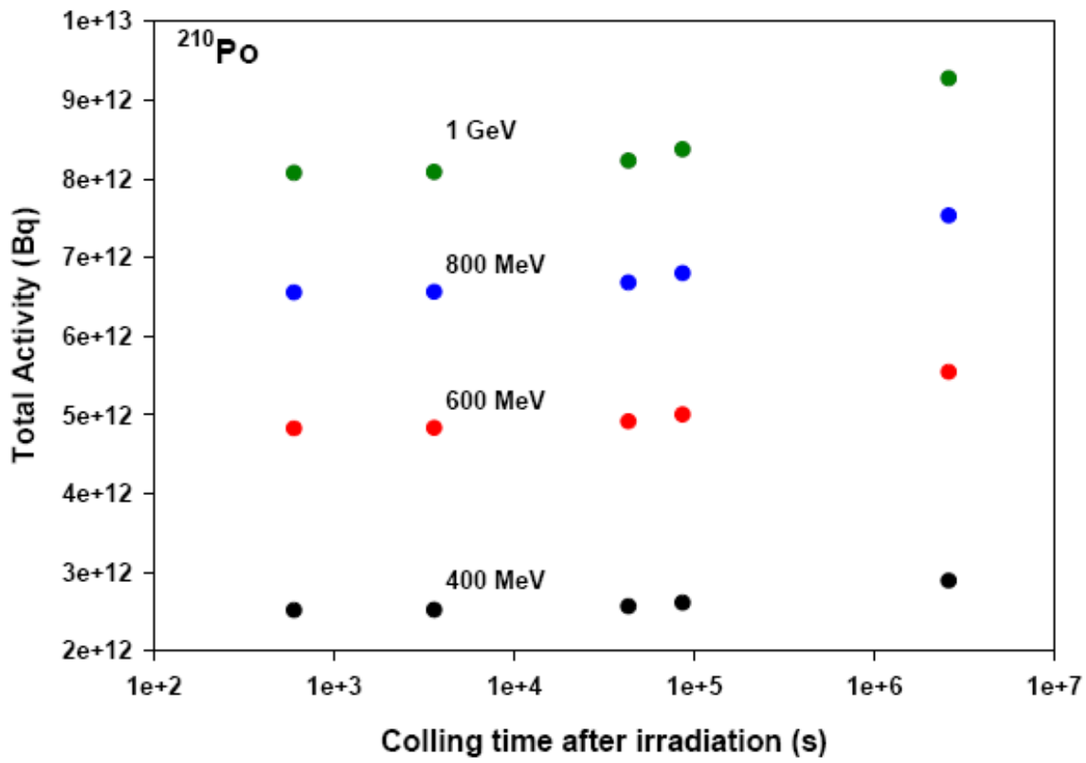

Fig. 7. Activity of ^{210}Po, produced from 1 mA proton beam irradiation of LBE target at different projectile energies, for 30 days, over different cooling times.

In the next part we report the induced activity in the window material made of T91 and D9 stainless steel. T91 and D9 are metal alloys used as the beam window in an ADSS facility. Isotopic composition of the window materials are given in section 2.1, Table 1. The window is not used as a stopping material, but only attenuates the beam. We have considered a thickness of 2.5 cm for the beam window. The build-up of radioactivity in T91 windows by proton induced reactions at beam energies of 400 MeV, 800 MeV and 1.2 GeV is shown in figures 8 (a), (b) and (c). From these figures we see that maximum activity is reached for ^{51}Cr of the order of $4.6\text{x}10^{13}$ Bq – $6.0\text{x}10^{13}$ Bq. The radioactivities produced for most of the other nuclides are in the range of 10^{11} Bq – 10^{12} Bq. Smallest activity is produced for ^{22}Na and ^{39}Ar in the range of 10^9 Bq – 10^{10} Bq. From these figures we see that for 30 days of irradiation, saturation activities are reached for ^{24}Na and ^{41}Ar. Gaseous radiotoxicity due to ^{3}H builds up from an activity of ~ 10^{11} - 10^{12} Bq and is much lower than the maximum activity produced.

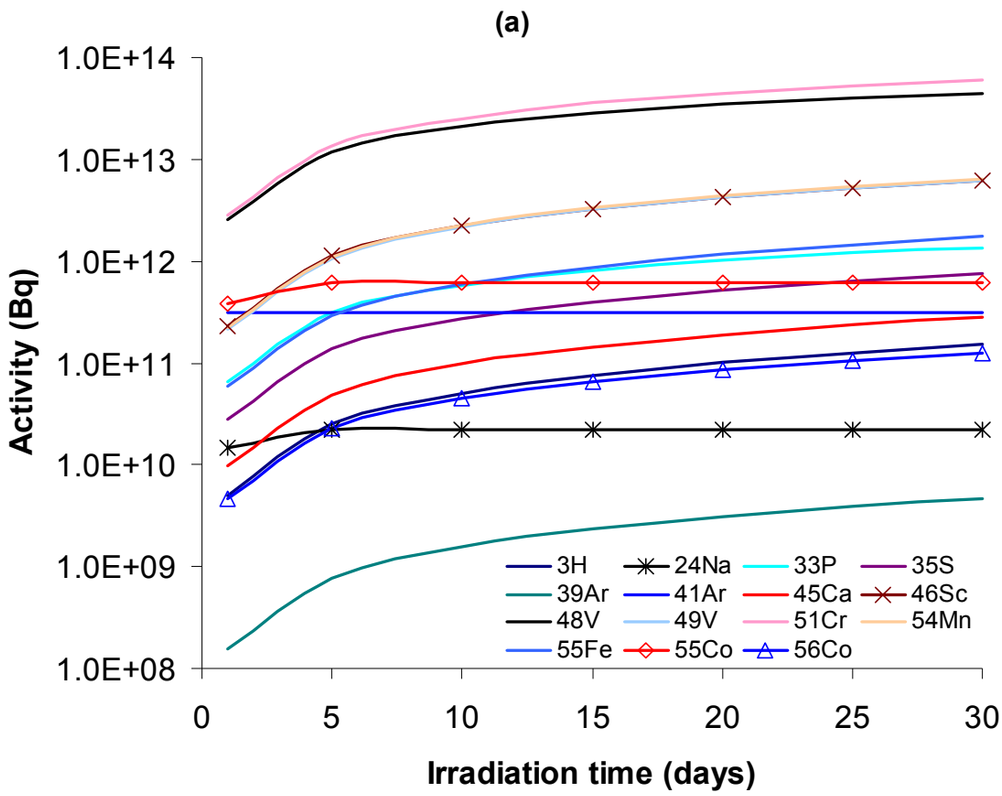
(a)
Activity (Bq)
1.0E+14
1.0E+13
1.0E+12
1.0E+11
1.0E+10
1.0E+09
1.0E+08
0
5
10
15
20
25
30
Irradiation time (days)
3H
24Na
33P
35S
39Ar
41Ar
45Ca
46Sc
48V
49V
51Cr
54Mn
55Fe
55Co
56Co

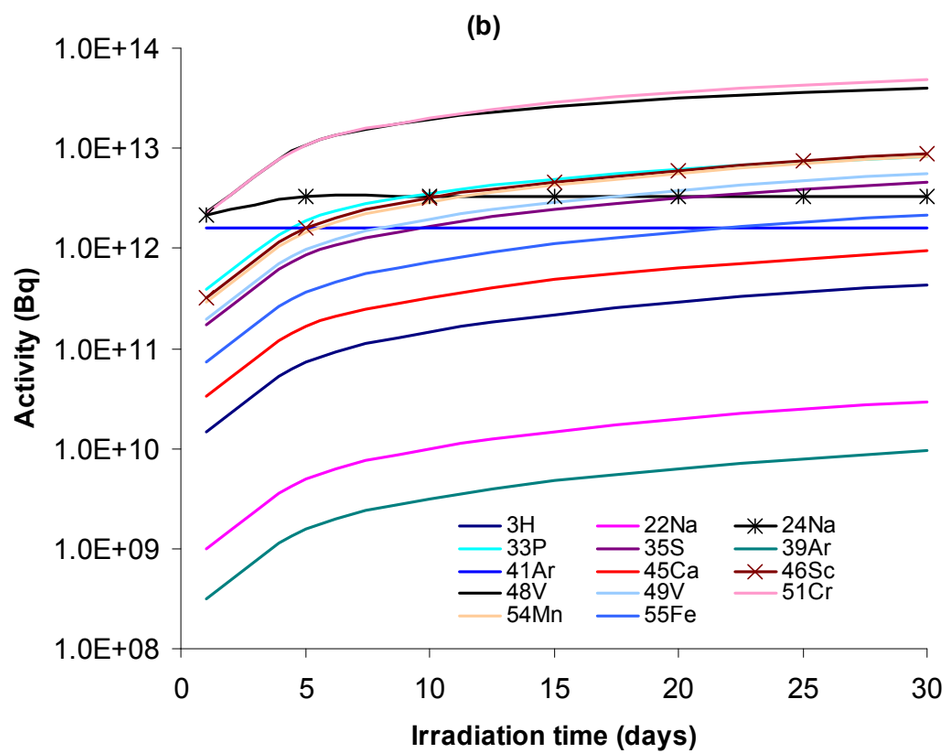
(b)
Activity (Bq)
1.0E+14
1.0E+13
1.0E+12
1.0E+11
1.0E+10
1.0E+09
1.0E+08
0
5
10
15
20
25
30
Irradiation time (days)
3H
22Na
24Na
33P
35S
39Ar
41Ar
45Ca
46Sc
48V
49V
51Cr
54Mn
55Fe

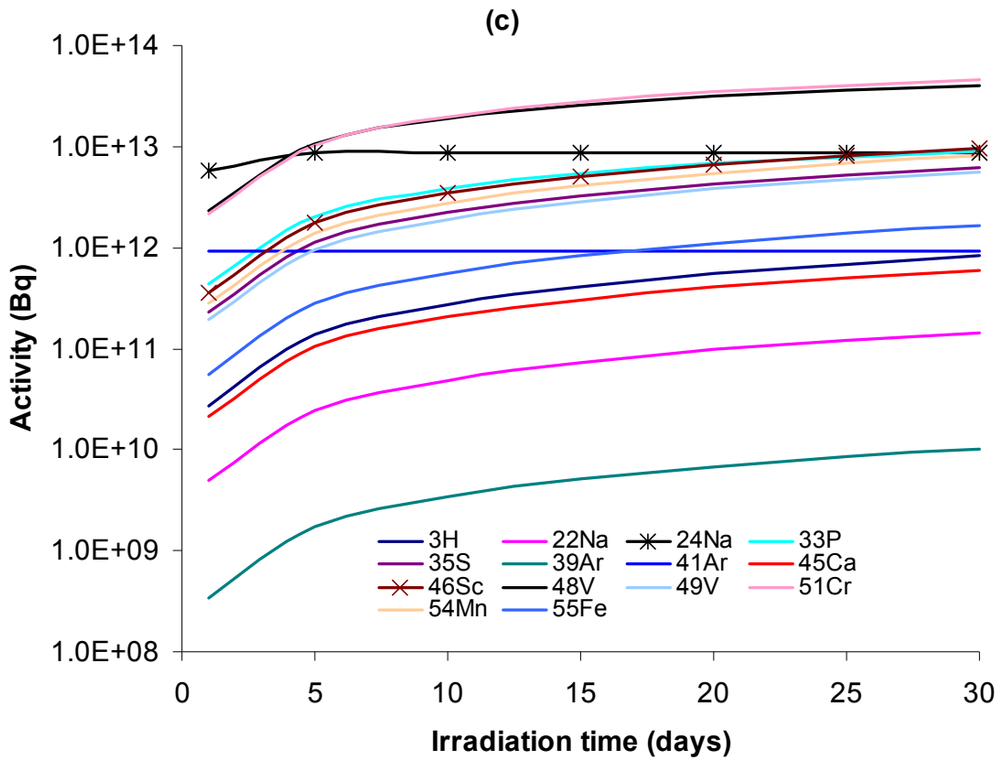

Fig. 8. Activity build-up of radionuclides in T91 window material for 1 mA proton beam induced reaction at beam energy of (a) 400 MeV, (b) 800 MeV and (c) 1.2 GeV

In figures 9 (a), (b) and (c) we have shown the build-up of radioactivity for the same radionuclides as in the case of T91 along with some additional nuclides produced in proton induced reactions on D9 at projectile energies of 400 MeV, 800 MeV and 1.2 GeV. The activity build-up pattern for different radionuclide species in this case is similar to that in the case of T91 target. In the case of D9 window we observe production of ^{60}Co for beam energies of 800 MeV and 1.2 GeV. Among the various radioisotopes studied for D9 window, ^{60}Co is produced with minimum activity, has a half-life of 5.27 years, has two strong characteristic γ-rays and hence is a source of potential hazard. Activity of ^{60}Co is produced in the range of 5.0×10^{8} Bq – 1.2×10^{9} Bq. Proper precautionary measure need be taken for handling these window materials.

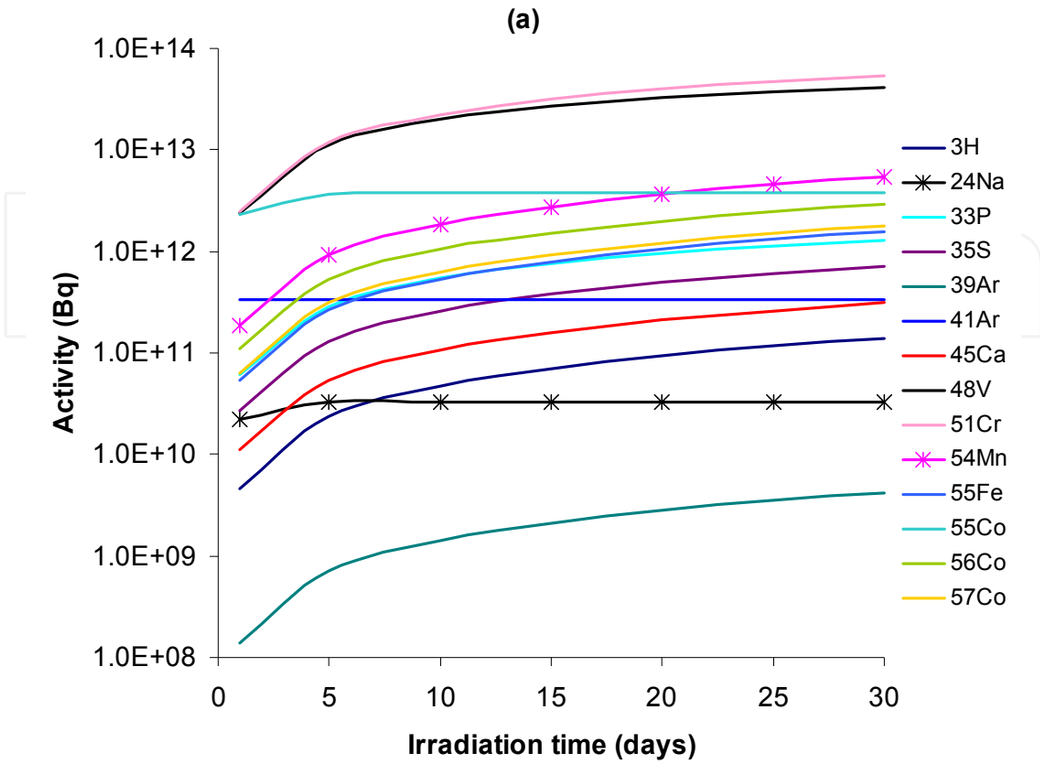
(a)
1.0E+14
1.0E+13
1.0E+12
1.0E+11
1.0E+10
1.0E+09
1.0E+08
Activity (Bq)
0
5
10
15
20
25
30
Irradiation time (days)
3H
24Na
33P
35S
39Ar
41Ar
45Ca
48V
51Cr
54Mn
55Fe
55Co
56Co
57Co

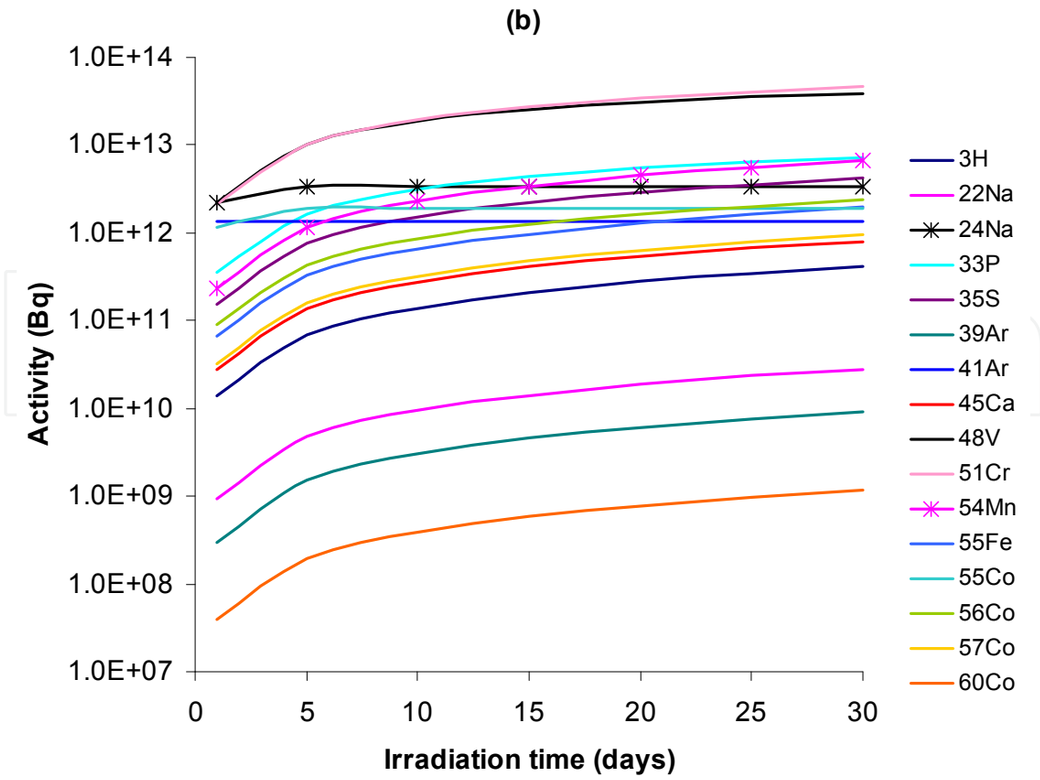
(b)
1.0E+14
1.0E+13
1.0E+12
1.0E+11
1.0E+10
1.0E+09
1.0E+08
1.0E+07
Activity (Bq)
0
5
10
15
20
25
30
Irradiation time (days)
3H
22Na
24Na
33P
35S
39Ar
41Ar
45Ca
48V
51Cr
54Mn
55Fe
55Co
56Co
57Co
60Co

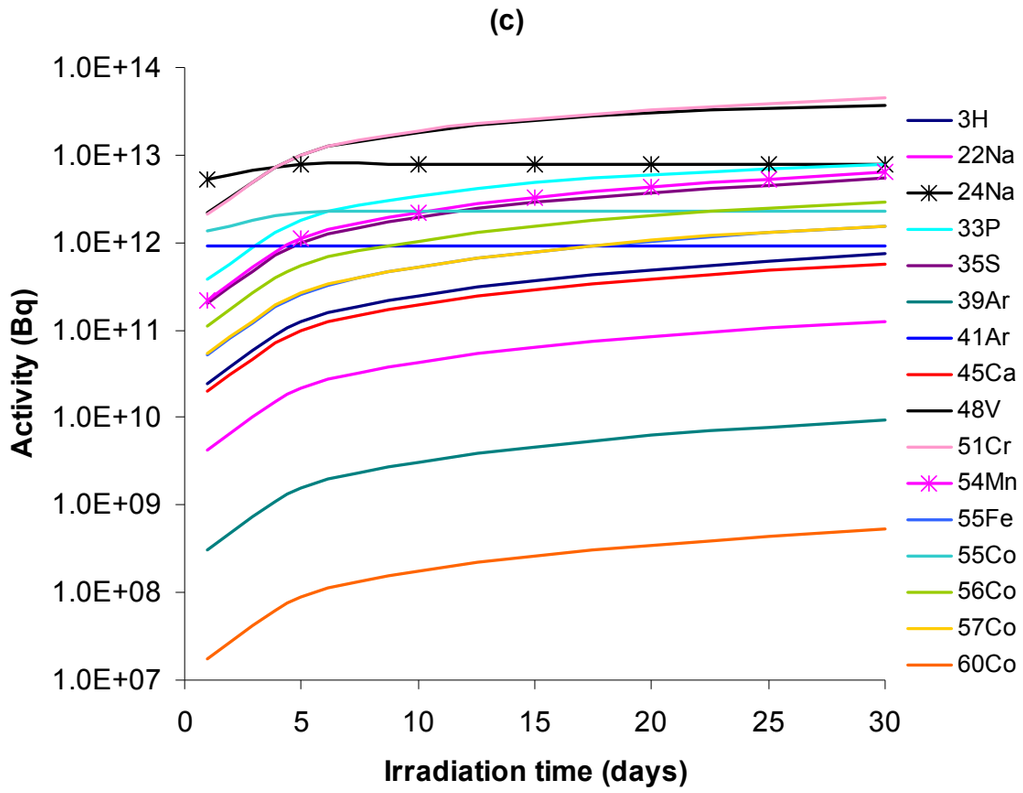

Fig. 9. Activity build-up of radionuclides in D9 window material for 1 mA proton beam induced reaction at beam energy of (a) 400 MeV, (b) 800 MeV and (c) 1.2 GeV

4. Conclusion

It has been observed from the analysis of the present work that a significant inventory of radiotoxic isotopes are produced due to irradiation of LBE target by protons in the energy range of 400 MeV to 1.2 GeV at a beam current of 1 mA. Highest yield of radioisotopes with high radiotoxicity like ^{3}H, ^{14}C, ^{22}Na, ^{60}Co, ^{203}Hg, ^{210}Po is obtained at 1.2 GeV proton energy and it has been observed that production of radiotoxic nuclides increases with increasing proton energy. This is undesirable, but on the other hand neutron yield increases with increasing proton energy, which is desirable. Thus a compromise has to be struck between

the two conflicting requirements. QMD calculations for 0.4, 1.2 and 2.0 GeV proton induced reactions on LBE target show that the ratio total neutron yield/total mass yield (which is an indicator of the neutron economy against radioactive waste generation) increases from ~8.0 at 0.4 GeV to 9.0 at 1.2 GeV and then decreases to ~8.36 at 2.0 GeV.

In an ADSS, a window is used to separate the beam transport pipe from the liquid metal target. T91 target window is known to perform better under severe stress to which the ADSS target window is subjected to and in handling the large amount of heat developed. Our study shows that the induced radioactivity in T91 window due to 1.2 GeV 1 mA proton beam is higher than that in D9 window by ~10% but is still preferred for its better performance under severe conditions [16].

Many of the radioisotopes produced are β– or β+ active and should be properly shielded against internal contamination along with the α emitters. Maximum activity is produced for ^{200,201}Tl and ^{203}Pb of the order of 6x10^7 MBq. Half-lives of these isotopes are of the order of 1-3 day and proper decay time may be allowed for these activities to cool down to the acceptable limit. ^{207}Bi, having a half-life of 31.55 years and characteristic γ-ray emissions with energies 0.569, 0.894 and 1.43 MeV, is produced with an activity of 10^4 MBq. Precautionary measure should be taken for handling of target assembly and disposal of used target with such long-lived activities. Total containment of induced activity during and after operation and proper waste disposal facility should be in place for efficient running of the ADS system. ^{210}Po activity, which is a potential source of α-contamination, is generated to the extent of ~ 8 – 9 x10^6 MBq. ^{3}H, which poses radiation hazard threat to the environment by adding to ground water contamination, is produced with an activity of 10^5 MBq from the irradiation of T91 and D9 beam windows. Proper containment for both ^{3}H and ^{210}Po should be ensured to protect plant personnel and environment from unwanted exposure to radiation while operating a target assembly containing a beam window.

In a high energy accelerator like one in ADSS, neutrons from the primary interaction contribute a significant fraction of the total radioisotope inventory. This should be taken into account while calculating the production cross section of the nuclides in the framework of QMD model. The inventory of radioisotopes presented in this work should provide an estimate of the total induced activity in such an ADSS facility using LBE target either with a beam window of stainless steel or a windowless target. Calculated values of induced activity will be scaled up by the ratio of currents if the system need be run at higher currents.

5. Acknowledgement

The authors gratefully acknowledge the support provided by Ms. C. Lahiri, presently at Physics Department, University of Calcutta, Kolkata, by assisting in a part of the calculations." should be replaced by "….part of the calculations and by CBAUNP project, SINP.

6. References

[1] A Letourneau *et al*, *Nucl. Instrum. Methods* B70, (2000) 299.
[2] Maitreyee Nandy and P.K. Sarkar, PRAMANA-Journal of Physics 61 (4) (2003) 675

[3] P. Vladimirov, A. Mslang, J. Nucl. Mater Part 1 329–333 (2004) 233.
[4] T. Obara, T. Miura, H. Sekimoto, Prog. Nucl. Energy 47 (1–4) (2005) 577; J. Zhang, N. Li, J. Nucl. Mater 326 (2–3) (2004) 201.
[5] Maitreyee Nandy and P.K. Sarkar, Nucl. Instr. Meth. Phys. Res. A 583 (2007) 248
[6] K Niita, S Chiba, T Maruyama, T Maruyama, H Takada, T Fukahori, Y Nakahara and A Iwamoto, *Phys. Rev.* C52, 2620 (1995); K Niita, T Maruyama, T Maruyama and A Iwamoto, *Prog. Theor. Phys.* 98, 87 (1997)
[7] A Fasso, et al FLUKA: a multi-particle transport code, (2005), CERN-2005-10.
[8] J.F. Ziegler, J.P. Biersack, U. Littmark, "The Stopping and Range of Ions in Solids", Pergamon Press, New York, 1985.
[9] M. Nandy, T. Bandyopadhyay, P.K. Sarkar, Phys. Rev. C 63 (2001) 034610.
[10] Sunil C., Maitreyee Nandy and P.K. Sarkar, Phys. Rev. C 78 (2008) 064607.
[11] http//www.nndc.bnl.gov, C,96MOSCOW, 221,96.
[12] http//www.nndc.bnl.gov, C,96SAROV,184,(1996).
[13] R.B. Firestone et al, "Table of Isotopes", ed. S.Y. Frank Chu, Coral M. Baglin, 8th edition, Lawrence Berkeley National Laboratory, University of California (1999)
[14] Anna Kowalczyk, "Proton induced spallation reactions in the energy range 0.1 - 10 GeV" arXiv:0801.0700v1 [nucl-th] 4 Jan 2008
[15] Y. Kadi * and J.P. Revol, "Design of an Accelerator-Driven System for the Destruction of Nuclear Waste", Workshop on Hybrid Nuclear Systems for Energy Production, Utilisation of Actinides & Transmutation of Long-Lived Radioactive Waste, Trieste, LNS0212002 3 - 7 September (2001)
[16] V. Mantha, A. K. Mohanty and P Satyamurthy, PRAMANA-Journal of Physics 68 (2) (2007) 355

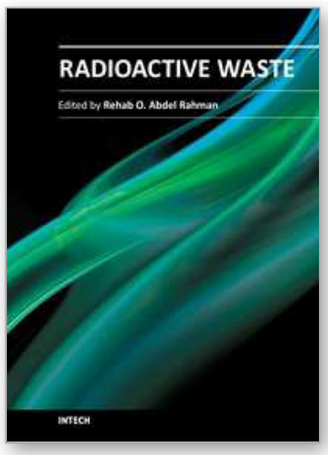

Radioactive Waste

Edited by Dr. Rehab Abdel Rahman

ISBN 978-953-51-0551-0
Hard cover, 502 pages
Publisher InTech
Published online 25, April, 2012
Published in print edition April, 2012

The safe management of nuclear and radioactive wastes is a subject that has recently received considerable recognition due to the huge volume of accumulative wastes and the increased public awareness of the hazards of these wastes. This book aims to cover the practice and research efforts that are currently conducted to deal with the technical difficulties in different radioactive waste management activities and to introduce to the non-technical factors that can affect the management practice. The collective contribution of esteem international experts has covered the science and technology of different management activities. The authors have introduced to the management system, illustrate how old management practices and radioactive accident can affect the environment and summarize the knowledge gained from current management practice and results of research efforts for using some innovative technologies in both pre-disposal and disposal activities.

InTech Europe
University Campus STeP Ri
Slavka Krautzeka 83/A
51000 Rijeka, Croatia
Phone: +385 (51) 770 447
Fax: +385 (51) 686 166
www.intechopen.com

InTech China
Unit 405, Office Block, Hotel Equatorial Shanghai
No.65, Yan An Road (West), Shanghai, 200040, China
中国上海市延安西路65号上海国际贵都大饭店办公楼405单元
Phone: +86-21-62489820
Fax: +86-21-62489821

IntechOpen